Lab on a Chip

Simultaneous biochemical and functional phenotyping of single circulating tumor cells using ultrahigh throughput and recovery microfluidic devices

Journal:	*Lab on a Chip*
Manuscript ID	LC-ART-05-2021-000454.R1
Article Type:	Paper
Date Submitted by the Author:	20-Jul-2021
Complete List of Authors:	Liu, Yang; University of Georgia, Chemistry Zhao, Wujun; FCS Technology, LLC Cheng, Rui; University of Georgia, School of Electrical and Computer Engineering Hodgson, Jamie; University Cancer & Blood Center, LLC Egan, Mary; University Cancer & Blood Center, LLC Pope, Christen; University Cancer & Blood Center, LLC Nikolinakos, Petros; University Cancer & Blood Center, LLC Mao, Leidong; University of Georgia, College of Engineering

Simultaneous biochemical and functional phenotyping of single circulating tumor cells using ultrahigh throughput and recovery microfluidic devices

Yang Liu,[a] Wujun Zhao,[b] Rui Cheng,[c] Jamie Hodgson,[d] Mary Egan,[d] Christen N. Cooper Pope,[d] Petros G. Nikolinakos,[d] and Leidong Mao*[c]

[a]Department of Chemistry, The University of Georgia, Athens, Georgia, USA

[b]FCS Technology, LLC, Athens, GA, 30606

[c]School of Electrical and Computer Engineering, College of Engineering, The University of Georgia, Athens, Georgia, USA.

[d]University Cancer & Blood Center, LLC, Athens, GA, 30607

*Email: Leidong Mao (mao@uga.edu)

†Electronic supplementary information (ESI) available.

Abstract

Profiling circulating tumour cells (CTCs) in cancer patients' blood samples is critical to understanding the complex and dynamic nature of metastasis. This task is challenged by the fact that CTCs are not only extremely rare in circulation but also highly heterogenous in their molecular programs and cellular functions. Here we report a combinational approach for the simultaneous biochemical and functional phenotyping of patient-derived CTCs, using an integrated inertial ferrohydrodynamic cell separation (i^2FCS) method and a single-cell microfluidic migration assay. This combinatorial approach offers unique capability to profile CTCs on the basis of their surface expression and migratory characteristics. We achieve this using the i^2FCS method that successfully processes whole blood samples in a tumor cell marker and size agnostic manner. i^2FCS method enables an ultrahigh blood sample processing throughput of up to 2×10^5 cells s^{-1} with a blood sample flow rate of 60 mL h^{-1}. Its short processing time (10 minutes for a 10 mL sample), together with a close-to-complete CTC recovery (99.70% recovery rate) and a low WBC contamination (4.07-log depletion of leukocytes), result in adequate and functional CTC for subsequent studies in the single-cell migration device. For the first time, we deploy this new approach to query CTCs with single-cell resolution in accordance with their expression of phenotypic surface markers and migration property, revealing the dynamic phenotypes and the existence of a high-motility subpopulation of CTCs in blood samples from metastatic lung cancer patients. This method could be adopted to study the biological and clinical values of invasive CTC phenotypes.

Introduction

Circulating tumor cells (CTCs) are implicated in the formation of metastatic tumors, which is responsible for as much as 90% of cancer-related mortality.[1-6] While the number of tumor cells in blood circulation correlated to clinical outcomes,[7-9] it has become clear that enumeration alone was not sufficient in understanding their multifaceted role in metastasis, in which CTCs participate in nearly all aspects of the process.[3, 10, 11] Cancer patients have CTCs of varying phenotypes in their blood circulation; [1, 4, 10, 12-15] while some cells passively detach themselves from the primary tumor,[16] a fraction of them gain the ability to actively invade distance organs through modifying their cellular programs, morphology and surrounding tissues.[17] Cells of this invasive phenotype often exhibit a high-motility trait that allow them to be efficient in hematological spread, thus possess the greatest threat of metastasis.[3, 10, 11, 18, 19] Despite rapid advances in the understanding of the molecular mechanisms of CTCs,[4, 13, 15] functional properties of invasive CTC phenotype remain poorly understood due to the limitations of existing CTC isolation and phenotyping methods.[20-22]

CTC's extreme scarcity in blood circulation (<10 CTCs per one milliliter of whole blood) and a lack of methods for the isolation of adequate and functional cells are the main bottleneck in studying the invasive phenotypes of CTCs.[20, 22] CTCs are highly heterogeneous in their biological and biophysical characteristics with multiple phenotypes co-existing, which can evolve dynamically over the course of metastasis.[3, 10, 11] Existing isolation techniques relying on the expression of tumor cell surface epitopes bias the sampling population and reduce the heterogeneity of captured cells.[20] These techniques also lead to immobilized and non-functional CTCs and limit possibility of conducting functional studies.[20] Physical property separation methods relying on size-based selection can separate larger CTCs from smaller leukocytes without limiting to molecular markers for selection. However, the isolated cells are contaminated with a large number of leukocytes and may also miss CTCs that were

morphologically similar to the leukocytes. As such, current microfluidic methods for invasiveness phenotyping of tumor cells were mostly confined to cultured cancer cells rather than patient-derived CTCs.[23-27] New methods are needed to isolate adequate and functional CTCs from patient samples so that the properties of invasive cells can be identified.

Here we report a novel combinational approach, which first uses an integrated inertial ferrohydrodynamic cell separation (i^2FCS) method to recover all CTCs from blood samples with minimal contamination in a tumor cell marker and size agnostic manner. Adequate and functional CTCs isolated from this method enable their biochemical and functional properties to be quantitatively profiled using a microfluidic assay that can track single tumor cell's chemotactic migration over time. In isolating CTCs when they are present at extremely low levels in the whole blood, we find that i^2FCS method enables an ultrahigh blood sample processing throughput of up to 2×10^5 cells s^{-1} with a sample flow rate of 60 mL h^{-1}, resulting in a 10 minutes device processing time for a standard 10 mL of blood sample. The short processing time, together with a close-to-complete CTC recovery rate of 99.70% and a low WBC contamination of ~507 WBCs carryover per milliliter blood processed, preserve isolated CTCs' viability and biological functions, allowing simultaneous biochemical and functional phenotyping of single tumor cells isolated from cancer patient's blood. Using this approach, we reveal a great diversity of biochemical and functional phenotypes of CTCs with single-cell resolution. CTCs with different levels of epithelial and mesenchymal marker expression exhibit varying chemotactic migration profiles, and there exists a high-motility subpopulation of CTCs in the patient's sample.

Results and discussion

Overview of the i^2FCS approach

The integrated inertial ferrohydrodynamic cell separation (i^2FCS) approach leverages the integration of cell size-based inertial focusing and cell magnetization-based ferrohydrodynamic separation (Figure 1a) for a tumor cell marker and size agnostic isolation. In this approach, mixture of red blood cells lysed blood sample from cancer patients with a colloidally stable magnetic fluid (ferrofluid) first flow through an inertial focusing stage, in which both tumor cells and blood cells are ordered into narrow streams in sigmoidal microchannels with alternating curvatures. The channel geometry and flow parameters in this stage enable the cells to experience inertial lift and Dean drag that force them to migrate to balanced locations within the curved channel (Figures 1a and 1e).[28-30] In the second stage of the approach, inertially-focused cell streams are ferrohydrodynamically separated into different spatial locations according to their magnetization difference. Its physical principle, illustrated in Figure 1b, shows that white blood cells (WBCs) are rendered magnetic by labeling of magnetic microbeads through a combination of leukocyte biomarkers, while CTCs remain unlabeled. Magnetization of the ferrofluid is fine-tuned to be less than that of WBC-bead conjugates, so that unlabeled CTCs with a close to zero magnetization, regardless of their size profiles, are collected via a magnetic field minima close to the boundary regions of the microchannel due to a phenomenon known as "diamagnetophoresis",[31] while WBC-bead conjugates are depleted via a magnetic field maxima at the channel center through a competition between both "magnetophoresis" and "diamagnetophoresis" (Figure 1e). The integration of inertial focusing and ferrohydrodynamic separation results in a compact microfluidic device with just one fluidic inlet and two fluidic outlets (Figure 1c), which can be operated using a single syringe pump for CTC isolation (Figure 1d).

Design principles of the i^2FCS approach

The i^{2}FCS approach was optimized to realize an isolation of functional CTCs in a tumor cell marker and size agnostic manner. Optimized i^{2}FCS devices have the following characteristics: (1) a complete isolation of CTCs from blood samples with 99.70% recovery rate; (2) an ultrahigh throughput of >600 millions of nucleated cells per hour (up to 200,000 cells s^{-1}) and a ultrahigh sample flow rate of 60 mL h^{-1}; (3) an extremely low carryover of ~507 WBCs for every 1 mL of blood processed; (4) isolated CTCs preserving their initial viability and functions and enabling their biochemical and functional analysis. These performance characteristics were realized through optimizing i^{2}FCS devices' geometry, magnetic field pattern, WBC functionalization, sample flow rate and ferrofluid concentration. A physical model that could predict the dynamics of cells in the i^{2}FCS devices was developed for the optimization process.[32, 33]

Firstly, the channel dimensions of both inertial focusing and ferrohydrodynamic separation stages in i^{2}FCS were designed to accommodate a high blood sample flow of 60 mL h^{-1}, which greatly reduced the device processing time of blood samples (10 minutes for a standard 10 mL blood sample). For the inertial focusing stage, we designed it so that both tumor and blood cells with diameters larger than 4 μm could be efficiently focused at a flow rate of 60 mL h^{-1}. The geometry of the inertial focusing stage was fine-tuned so that the particle Reynolds number (R_p) was 5.4, and the channel Reynolds number (R_c) was 51.5 when the flow rate was 60 mL h^{-1}, ensuring a well-focused cell stream (~100 μm in width) before the ferrohydrodynamic separation stage. For the ferrohydrodynamic separation stage, the channel dimension (54.8 × 1.2 × 0.06 mm, *length* × *width* × *height*) was optimized so that the channel Reynold's number was 21.3 when the sample flow rate was 60 mL h^{-1}, ensuring unperturbed laminar flow conditions during CTC isolation. Secondly, we designed the generation of magnetic fields in i^{2}FCS with a sextupole magnet configuration (Figure 2) to obtain a significant magnetic force on the cells for efficient cell separation. A magnetic flux density of

up to 3.2 T (1.1 – 1.4 T within the ferrohydrodynamic separation channel) (Figures 2a-d) and a gradient of magnetic flux of up to 670 T m^{-1} (Figure 2e) were obtained from the sextupole configuration. As shown in Figures 2b and 2d, the magnetic flux density was maximal at the center of the separation microchannel, while the absolute value of the flux density gradient was minimal. Using this magnetic field pattern, the directions of the magnetophoretic WBCs and diamagnetophoretic CTCs in the microchannel are opposite to each other, eliminating the need of sheath flow in i^2FCS devices and simplifying the device's fluidic operation. Thirdly, we optimized the WBC functionalization by using a combination of five leukocyte biomarkers (CD45, CD45RA, CD66b, CD16, and CD3).34 Biotinylated biomarker antibodies were labeled with the WBCs then conjugated with streptavidin-coated Dynabeads (1.05 μm diameter, 11.4% volume fraction of magnetic materials). The use of five markers allowed us to reduce the number of Dynabeads per WBC (20 per cell), because on average streptavidin-coated Dynabeads had a high probability of conjugating to WBCs due to the increased presence of biotins from the five markers. In our experiences, unconjugated Dynabeads tended to clog microchannels under strong magnetic field gradients. Therefore, the decreased use of Dynabeads in this method resulted in the elimination of microchannel clogging issues. With this labeling protocol, WBCs were conjugated with 21 ± 9 (mean ± s.d.) beads and >99.95% of WBCs were labeled with at least two beads (Figures 3a, left). Based on the number of beads on the WBCs and corresponding cell size, we calculated the upper bound of the magnetic volume fraction of the ferrofluid to deplete WBCs. Lastly, we studied the effects of ferrofluid concentration and blood sample flow rate on the separation performance in the above-mentioned physical model. Simulated cells' position (denoted as Y) and separation distance between WBCs and tumor cells at the device outlets (denoted as ΔY) on the ferrofluid concentration and sample flow rate are shown in Figures 3c and 3d. Maximal separation distance occurred when the ferrofluid concentration is 0.015% (Figure 3c) and the flow rate

was 1000 μL min^{-1} or 60 mL h^{-1} (Figure 3d). Using these optimized parameters (ferrofluid concentration: 0.015% (v/v); flow rate: 1000 μL min^{-1} or 60 mL h^{-1}), positions of 10,000 MCF7 cancer cells and 10,000 labeled WBCs at the outlet of the device were simulated and shown in Figure 3e. 100% of the MCF7 breast cancer cells are deflected toward the channel walls and are collected from the CTCs outlet of the device (Figure 3f), while approximately 99.95% of WBCs are depleted through the WBCs outlet (Figure 3g).

Throughput, recovery, purity and biocompatibility of the i^2FCS approach

Using the optimized i^2FCS device and operating parameters, we validated it with spiked cancer cells from a total of 11 cultured cancer cell lines, including 4 breast cancer cell lines (MCF7, MDA-MB-231, HCC1806, HCC70), 4 non-small cell lung cancer cell lines (A549, H1299, H3122, H520), 2 small cell lung cancer cell lines (DMS79, H69), and 1 prostate cancer cell line (PC-3). We evaluated the performance of i^2FCS in the cancer cells isolation, including sample flow rate and cell-processing throughput, cell recovery rate, WBC contamination, viability and proliferation of isolated cells. Figure 3i shows a typical separation process, in which ~100 MCF7 breast cancer cells stained with green fluorescence were spiked into 1 mL of WBCs (~6 million cells/mL) and processed at a flow rate of 60 mL h^{-1}. Cancer cells and WBCs were distinctively separated into different streams at the outlets of the device. No channel clogging due to magnetic beads was observed during the device operation of processing up to 600 millions of nucleated cells with a throughput of 100,000 cells s^{-1} and a flow rate of 60 mL h^{-1}. The throughput and flow rate of i^2FCS are approximately one order of magnitude higher than most existing CTC isolation methods (see supplementary information). The ultrahigh throughput of i^2FCS enables processing a typical blood sample of 10 mL in 10 minutes, significantly reducing chances of cell apoptosis during the device operation. We further characterized the performance of i^2FCS in recovering spiked cancer cells at clinical

concentrations (10 – 200 cells mL^{-1}). MCF7 breast cancer cells with spike ratios ranging from 10 to 200 cells per mL were recovered using the devices at a recovery rate of 100% with minimal variations (n = 3, Figure 4a), indicating i^2FCS's ability to completely recover spiked cancer cells at clinical concentrations. We further challenged the device with 10 additional cancer cell lines with distinct size profiles (Figure 4b). i^2FCS showed close-to-complete recovery rates across all cancer cell lines used in this study (100.00 ± 0.00%, 99.33 ± 0.49%, 99.67 ± 0.47%, 99.83 ± 0.24%, 99.67 ± 0.47%, 99.67 ± 0.42%, 100 ± 0.00%, 100 ± 0.00%, 100 ± 0.00%, 99.67 ± 0.94%, and 98.83 ± 1.03% for MCF7, MDA-MB-231, HCC1806, HCC70, A549, H1299, H3122, H520, DMS79, H69, and PC-3 cell lines, mean ± s.d., n = 3 for each cell line) (Figure 4c). The average recovery rate across 11 cancer cell lines was 99.70 ± 0.34% (mean ± s.d., n = 11), including the small cell lung cancer cells (DMS79 and H69). The recovery rate of i^2FCS device is higher than other microfluidic approaches (see supplementary information), including the CTC-iChip.[35, 36]. Current range of cell concentration processed by i^2FCS was 3 – 20 millions cells/mL. Higher cellular concentration would slightly decrease the cancer cell recovery rate (see supplementary information). i^2FCS also greatly reduced the contamination of WBCs. The i^2FCS device achieved 4.07-log depletion of WBCs by removing 99.992% of the leukocytes from the blood samples, with approximately 507 ± 53 (mean ± s.d., n = 3) cells carryover in the CTC collection outlet after processing 1 mL of blood (Figure 4d). The majority of WBC contamination were WBCs labeled with ≤ 1 magnetic bead. The level of WBC contamination found in i^2FCS device is significantly lower than the majority of other microfluidic approaches (see supplementary information), and is comparable to the CTC-iChip approach.[35, 36] Lastly, we investigated the effect of the device processing on the cells' viability and proliferation. The combination of low ferrofluid concentration (0.015% of magnetic content by volume) and laminar flow conditions in the i^2FCS device showed little impact on the viability, intactness and proliferation of the isolated cancer cells. Figure 4e shows that cell

viabilities of H1299 lung cancer cells before and after i^{2}FCS processing were 99.31 ± 0.42% and 98.10 ± 1.35 % (mean ± s.d., n = 3), respectively, indicating a negligible device effect on the cell viability. Fluorescence images of live/dead assay in Figure 4f show the viability and intactness of the cancer cells were well preserved after the device processing. The isolated cancer cells continued to proliferate into confluence after 48 hours' culture (Figure 4f), with unaffected marker expressions on their surface (Figure 4g).

Biochemical phenotyping of CTCs in cancer patients

To evaluate the performance of i^{2}FCS in isolating heterogeneous CTCs in clinical samples, we conducted a study of samples collected from 2 patients exhibiting stage IV metastatic non-small cell lung cancer. Immunofluorescent staining was used to distinguish CTCs and WBCs, and CTCs of different phenotypes. We used the i^{2}FCS devices to process blood samples from the patients, who were recruited and consented at the University Cancer and Blood Center (Athens, Georgia) under an approved IRB protocol (University of Georgia, VERSION00000869). Surface markers corresponding to epithelial and mesenchymal phenotypes were chosen because CTCs are reported to go through EMT, epithelial to mesenchymal transition, in which original epithelial tumor cells transition into stem-like mesenchymal cells.[10, 11, 37] The loss of epithelial characteristics and the acquisition of mesenchymal characteristics are closely linked to the tumor cells' high motility and invasiveness to create a new tumor site.[10, 37-39] CTCs of this functional phenotype are therefore the focus of this study. 20 mL of blood sample from each patient was processed by the i^{2}FCS devices. A quarter of the isolated cells were used for biochemical phenotyping through immunofluorescent staining with an epithelial marker (EpCAM) that is downregulated in EMT,[20, 37, 38] two mesenchymal markers (vimentin and N-cadherin) that are upregulated in EMT, [18, 37, 38] a leukocyte marker (CD45), and a nucleus marker (DAPI) for their identification. WBCs were identified as CD45 positive and DAPI positive (EpCAM–/Vim–/N-

cad–/CD45+/DAPI+). CD45 negative and DAPI positive CTCs were classified into three different phenotypes including epithelial phenotype (EpCAM+/Vim–/N-cad–), mesenchymal phenotype (EpCAM–/Vim+/N-cad–, EpCAM–/Vim–/N-cad+, or EpCAM–/Vim+/N-cad+), and mixed epithelial and mesenchymal phenotype (EpCAM+/Vim+/N-cad– or EpCAM+/Vim+/N-cad+).

Examples of isolated CTCs are shown in Figure 5a. We first note that a significant number of CTCs were isolated from both patients' blood samples. 796 cells were identified as CTCs from patient A in a 5 mL volume of blood sample at a concentration of 159 CTCs/mL of blood sample, and 1262 were identified in patient B' sample (5 mL blood, 252 CTCs/mL concentration). The high counts of CTCs could be explained by the disease stages (stage IV metastatic non-small cell lung cancers) of both patients and the ability of i^2FCS to completely recover CTCs from blood. For verification purpose, a blood sample from a third patient (patient C, stage IV lung cancer) was processed by both i^2FCS and a recently reported size-selection method (inertial-FCS),[40] both of which yielded similarly high counts of CTCs (see supplementary information). Isolated CTCs from both patients were intact, indicating a minimal impact of the device processing on the cells' morphology. Consistent with previous reports,[32, 41-46] the effective cell diameter of isolated CTCs, defined as the maximum Feret diameter of the cells under bright-field imaging, showed a high level of variation for both patients. The effective diameters of randomly selected (n = 75) CTCs from patient A's sample were 13.29 ± 6.13 μm (mean ± s.d.), with the smallest diameter being 5.88 μm and the largest being 33.74 μm (Figure 5b). For patient B, the effective diameters of randomly selected CTCs (n = 70) were 10.22 ± 4.85 μm (mean ± s.d.), where the smallest diameter was 4.28 μm and the largest was 30.51 μm (Figure 5b). While the clinical relevance of CTCs with varying sizes is unclear, some consider that cells switching from an active state to a dormant state may be the cause of their size variation, which could contribute to their metastatic potential.[43]

Nonetheless, the polydispersity of isolated cells highlights the effectiveness of the cell size agnostic i^{2}FCS approach in recovering CTCs that are comparable in size to WBCs, enabling downstream studies on these cells. We further characterized the biochemical phenotypes of the isolated CTCs through their surface antigen expression using the above-mentioned epithelial and mesenchymal markers. The proportion of each phenotypic subtypes of CTCs are summarized in Figure 5c, which shows interesting comparison between two patients. Isolated CTCs of patient A had a significant portion of epithelial phenotype (64.8% EpCAM+/Vim–/N-cad–) while patient B's CTCs had a predominately mesenchymal phenotype (40.3% EpCAM–/Vim+/N-cad+, 20.6% EpCAM–/Vim–/N-cad+, and 0.1% EpCAM–/Vim+/N-cad–), indicating that the majority of Patient B's cells have gone through the EMT. Patient A also presented 25.6% mesenchymal CTCs (15.6% of EpCAM–/Vim+/N-cad+, and 10.0% of EpCAM–/Vim–/N-cad+) in addition to the epithelial phenotype. Patient B presented 22.0 % of epithelial CTCs (EpCAM–/Vim+/ N-cad) in addition to the mesenchymal phenotype. Both patients had a relatively small percentage of CTCs that presented mixed epithelial and mesenchymal phenotypes (Patient A: 7.5% EpCAM+/Vim+/N-cad– and 2.1% EpCAM+/Vim+/N-cad+; Patient B: 4.9% EpCAM+/Vim+/N-cad– and 10.1% EpCAM+/Vim+/N-cad+, Figure 5c). The cells with mixed epithelial and mesenchymal phenotypes likely represented CTCs that were in transition between epithelial and mesenchymal status, indicating their evolution to more invasive phenotypes. Overall, the heterogeneity of biomarker expressions of isolated CTCs from these patients is consistent with previous reports and highlights the maker agnostic isolation of i^{2}FCS approach. CTCs of mesenchymal phenotype are reported to possess high motility and are more invasiveness than the epithelial phenotype.[10, 37-39] Therefore identifying the invasive subtype of CTCs with high motility is the focus of the subsequent functional study.

Functional phenotyping of CTCs in cancer patients

Adequate and functional CTCs isolated from the i^{2}FCS approach enable their simultaneous biochemical and functional phenotyping. In this study, we accessed how CTC subpopulations with different levels of epithelial and mesenchymal marker expression affect their chemotactic migration. We chose cell migration to access CTCs' functions because high motility of these cells are implicated in the metastatic spread, including local invasion into surrounding stroma and intravasation into blood circulation, extravasation into parenchyma of foreign tissue, colonization and formation of metastatic lesions.[3, 10, 11, 18, 19] The identification of high-motility CTCs would facilitate the prediction of a patient's risk of developing metastasis and the design of personalized therapeutics. i^{2}FCS's ultrahigh recovery rate allows us to isolate all CTCs from the patient samples, which potentially contain a subpopulation of these highly motile CTCs. In order to identify this subpopulation, we developed a new microfluidic assay that tracked cells' chemotactic migration with single cell resolution over a 24-hour period in confined microchannels.

CTC isolation and migration characterization process is shown in Figure 6a. A 20 mL of blood sample from Patient B was first processed by the i^{2}FCS device to isolate CTCs. Patient A's sample experienced a delay in its processing and was not included in the migration study. The isolated cells from Patient B were divided into three portions, with one quarter of the cells used for biochemical phenotyping through immunofluorescent staining (described in the previous section), and one quarter for the microfluidic migration assay. The remaining one half of cells was preserved for future studies. In constructing the microfluidic device and assay for CTCs' migration phenotyping, we applied the following design principles. Firstly, we chose to use chemotactic migration to guide CTC's migratory direction in the microfluidic assay because CTCs are most efficient when the cell is involved in directed migration.[47, 48] We used a spatial gradient of growth factors including epidermal growth factor (EGF), basic fibroblast growth factor (bFGF) and fetal bovine serum (FBS), to guide CTCs' migration in the

microchannels,[49] and a spatial gradient of Slit2 to inhibit the migration of carryover WBCs.[50, 51] The gradient of growth factors were maintained via a continuous perfusion for a 24-hour period in the microchannel to enable chemotactic migration of CTCs (Figure 6b). Secondly, we constructed microchannels to recapitulate the confined space through which tumor cells infiltrate organs *in vivo*.[19, 52-54] A total of 5,000 single cell migration tracks were packed in the device for CTCs to migrate, with each track having a cross-section of 30 μm (width) by 5 μm (height) and a total length of 1200 μm (Figure 6b), close to the dimensions of the tunnel-like tracks CTCs encountered in the extracellular matrix (ECM) of the tumor stroma.[19, 52-54] The single cell tracks were periodically interrupted to enable collection of migrated cells at the end of the experiments. This assay was first validated using H1299 lung cancer cells to show that it could differentiate migratory versus non-migratory subtypes (Figure 6c). In experiments using patient-derived CTCs, cells isolated from Patient B using an i^{2}FCS device were seeded in the microfluidic migration device at the loading channel, and allowed to migrate along the growth factors' gradient for 24 hours with incubation conditions of 37 °C and 5% CO_2. At the end of the 24-hour period, migratory cells were immunofluorescently stained within the device with an epithelial marker (EpCAM), a mesenchymal marker (Vimentin, Vim), a leukocyte marker (CD45) and a nucleus marker (DAPI) to identify their cell types. Migratory distance and speed of each identified CTCs (EpCAM+/Vim–/CD45–/DAPI+, EpCAM–/Vim+/CD45–/DAPI+, or EpCAM+/Vim+/CD45–/DAPI+) in the single cell tracks were recorded and analyzed.

We estimated that a total ~1260 CTCs isolated from 10 mL of blood sample were seeded in the microfluidic migration device at the start of the migration assay. The number of CTCs was calculated from the 252 CTCs/mL concentration obtained through immunochemistry for Patient B' sample. At the end of the 24-hour migration assay, we identified again through immunochemistry that a small percentage of initial CTCs (16.4%, 207

out of the 1260 seeded cells) remained in the migration device and exhibited chemotactic migration towards the growth factors' gradient. The other 83.6% of CTCs were likely apoptotic and washed away by the perfusion within the assay timeframe. Figures 6d-f summarize the distributions of final migratory position, migration speed and surface marker expression of the high-motility cell subpopulation. The migration speed of individual cells was calculated from the distance migrated (difference between initial and final positions within the microchannel) within 24 hours. These high-motility cells exhibited variable levels of migration during the 24-hour period, with a mean speed (Figure 6e) of 0.26 ± 0.19 μm min^{-1} (mean ± s.d., n = 207). This speed indicated that the migratory CTCs likely utilized the mesenchymal locomotion in the microchannels, which was reported to have a speed range of 0.1-1 μm min^{-1}.[55] We also observed that cells with a faster migratory speed and a longer migratory distance tended to have elongated cell morphology, while cells with a slower migratory speed and a shorter migratory distance had a mostly rounded shape (Figures 6f-g), consistent with previous findings of mesenchymal migration.[56, 57] Through the single-cell migration assay, we identified a subpopulation of CTCs from Patient B's sample that possessed high motility towards the gradient of growth factors. This subtype of high-motility CTCs exhibits different levels of epithelial and mesenchymal marker expressions and varying chemotactic migration property. The identification of these high-motility CTCs could enable further molecular and functional studies on them.

Comparison of i^{2}FCS to existing CTC enrichment methods

We objectively evaluated i^{2}FCS's performance in CTC separation to existing methods, using four commonly used metrics in calibrating CTC isolation methods, including the cell-processing throughput, CTC recovery rate, WBC contamination or carryover at device output and integrity of enriched cells. i^{2}FCS method reported an ultrahigh blood sample processing throughput of up to 2×10^5 cells s^{-1} with a blood sample flow rate of 60 mL h^{-1}. It resulted in a

close-to-complete recovery of spiked cancer cells (99.70% recovery rate) and an ultralow WBC contamination (4.07-log depletion of leukocytes, removing 99.992% of the leukocytes from the blood samples, with approximately 507 WBC carryover per 1 mL of processed blood). The short processing time of i^{2}FCS (10 minutes for 10 mL of blood) and complete recovery of CTCs produced adequate, viable and functional cells for subsequent cell-migration studies. We compared iFCS's performance to a total of 49 recently published CTC separation methods (see supplementary information) and found that i^{2}FCS had better overall performance in the above-mentioned four metrics than existing methods.

We also compared the performance of i^{2}FCS to two generations of CTC-iChip in Table 1.35, 36 i^{2}FCS had six times higher blood sample flow rate (60 mL h^{-1} for i^{2}FCS versus 10 mL h^{-1} for monolithic CTC-iChip). Both i^{2}FCS and CTC-iChip depleted roughly the same amount of WBCs from blood samples (507 cells/mL carryover for i^{2}FCS versus 445 cells/mL carryover for monolithic CTC-iChip). While the reported cancer cells recovery rates were almost the same for i^{2}FCS and CTC-iChip using spiked cancer cells (99.7% for i^{2}FCS versus 99.5% for monolithic CTC-iChip), the recovered CTCs from patient samples showed different physical diameter ranges, with i^{2}FCS being able to isolate patient CTCs with a broader physical diameter range than CTC-iChip (4.3 – 33.7 μm for i^{2}FCS versus 5.5 – 27 μm for monolithic CTC-iChip). i^{2}FCS has an advantage of being able to recover small CTCs, because it does not differentiate CTCs and blood cells based on their physical diameters. Instead it uses the contrast of cellular magnetization for separation. This working principle ensured that all CTCs were separated regardless of their diameters. On the other hand, CTC-iChip integrated deterministic lateral displacement (DLD) to deplete red blood cells, inertial focusing to concentrate nucleated cells, and magnetophoresis to separate magnetically labeled CTCs. The size-based DLD stage in CTC-iChip could potentially remove small CTCs of similar size to red blood cells (6–8 μm). This slight selection bias might explain the diameter difference in recovered CTCs between the

two methods. Finally, CTC-iChip could process whole blood without lysis while i^{2}FCS needed red blood cell lysis. Even though the cancer cell loss due to lysis step was demonstrated to be negligibly small (~0.08%) in cancer cell line control experiments,32 it would be difficult to characterize such CTC loss in patient samples. In summary, i^{2}FCS had the advantages of higher cell-processing throughput and sample flow rate, recovering CTCs with broader physical diameters, but lacked the ability to process whole blood when comparing to CTC-iChip.

Conclusion

We reported an integrated method that allowed for the first time simultaneous biochemical and functional phenotyping of patient-derived single circulating tumor cells. The method leveraged an integrated inertial ferrohydrodynamic cell separation (i^{2}FCS) approach for a tumor cell marker and size agnostic isolation of CTCs from patient samples. This approach yielded remarkable CTC isolation performance including a complete isolation of CTCs from blood samples with a 99.70% recovery rate, an ultrahigh throughput of >600 millions of nucleated cells per hour, a ultrahigh blood processing flow rate of 60 mL h^{-1}, and an extremely low carryover of ~507 WBCs for every one milliliter of blood processed. Furthermore, isolated CTCs from i^{2}FCS preserved their functional properties and enabled their biochemical and functional phenotypes to be quantitively queried via a single cell migration assay.

In samples collected from two metastatic lung cancer patients, i^{2}FCS and the migration assay enabled the sensitive profiling of CTCs' heterogeneity according to their surface antigen levels and migration phenotypes. CTCs profiled in samples collected from the patients revealed that there was a great level of diversity in the phenotypes of CTCs. CTCs exhibited variable levels of epithelial and mesenchymal antigen expressions and morphologies, confirming the marker and size agnostic isolation of the approach. Isolated cells were accessed for their motility towards a gradient of growth factors in a migration assay with single-cell resolution, revealing the existence of a high-motility subpopulation of CTCs in one of the patients' sample.

The i^{2}FCS and migration assay approach could be potentially adapted to a variety of applications in cancer research. CTCs isolated from the i^{2}FCS can readily be recovered with intactness and preserved biological functions, therefore facilitating further downstream analysis and culture. This approach allows multiplexed queries of functional CTCs, which makes it possible to analyze CTCs for their complex roles in metastasis. Experiments using this approach can be implemented using a standard syringe pump with microfluidic devices that are straightforward to fabricate and operate, making it relatively easy for laboratory adoptions.

Experimental section

Modeling and simulation

Magnetic field and particle separation performance was simulated and optimized in MATLAB (MathWorks, Natick, MA) using a physical model, which predicted trajectories of cancer cells and labeled WBCs in the microfluidic channel coupled with a sextupole configuration of magnets.[32, 33]

Microfluidic device fabrication

The master mold containing the microfluidic structures was fabricated using standing photolithography methods with SU-8 2025 photoresist (Kayaku Advanced materials, Westborough, MA). The height of the structures was measured to be 60 μm. The 1 mm thick PDMS layer was prepared with Sylgard 184 silicone elastomer kit (Ellsworth Adhesives, Germantown, WI) in a 1:7 ratio of cross-linker and base, and cured at 60 °C for 4 hours. After bonding with the inlet and outlet layer (5 mm thick PDMS), the devices were oven baked at 80 °C for 20 minutes following by a hotplate at 150 °C for 1 hour. The device was placed within a custom aluminum manifold that held six N52 NdFeB permanent magnets (K&J Magnetics, Pipersville, PA) in a sextupole configuration. The magnets had a geometry of 50.8 mm × 6.35 mm × 6.35 mm (L × W × H) and had a remanent magnetization of 1.48T each. Before each use, the devices were sterilized with 70% ethanol and then primed with 1× PBS supplemented with 0.5% (w/v) BSA and 2 mM EDTA (Thermo Fisher Scientific, Waltham, MA).

Ferrofluid synthesis and characterization

The water-based ferrofluid was a colloidal suspension of maghemite nanoparticles, synthesized by a chemical co-precipitation method following developed protocol.[58, 59] The saturation magnetization (1,107 A m^{-1}) and volume fraction of the ferrofluid (0.298%, v/v) were measured by a vibrating sample magnetometer (VSM, MicroSense, Lowell, MA). The

viscosity of the ferrofluid (1.7 mPa s^{-1}) was characterized via a compact rheometer (Anton Paar, Ashland, VA) at room temperature. The diameter and morphology of maghemite nanoparticles were determined to be 10.91 ± 4.87 nm (mean ± s.d.) with a transmission electron microscopy (TEM; FEI, Eindhoven, the Netherlands).

Cell culture and preparation

11 human cancer cell lines including four breast cancer cell lines (MCF7, MDA-MB-231, HCC1806, and HCC70), four non-small cell lung cancer (NSCLC) cell lines (A549, H1299, H3122, and H520), two small cell lung cancer (SCLC) cell lines (DMS79 and H59) and one prostate cancer cell line (PC-3) were purchased from ATCC (Manassas, VA). Cell cultures followed the manufacturing instructions. Breast cancer cell lines MCF7 and MDA-MB-231 were cultured in DMEM medium (Thermo Fisher Scientific, Waltham, MA) and the other cell lines were cultured in RPM 1640 medium (Thermo Fisher Scientific, Waltham, MA). DMEM and RPMI medium were supplemented with 10% (v/v) fetal bovine serum (FBS, Thermo Fisher Scientific, Waltham, MA), 1% (v/v) penicillin/streptomycin solution (Thermo Fisher Scientific, Waltham, MA), and 0.1 mM non-essential amino acid (NEAA, Thermo Fisher Scientific, Waltham, MA). All the cell lines were cultured at 37 °C with 5% CO_2. When the cells grown into 80% confluence, cells were washed twice with PBS by gently shaking the cell culture flask. This step was required to remove dead cells and debris. Cells were released with 0.05% trypsin-EDTA solution (Thermo Fisher Scientific, Waltham, MA), centrifugated (5 min, 500g) to remove the supernatant, and resuspend in 1× Dulbecco's Phosphate Buffered Saline (DPBS, Thermo Fisher Scientific, Waltham, MA). To track the cell trajectories in the i^2FCS device, cells were either stained with 3 μM CellTracker Green or 3 μM CellTracker Orange (Thermo Fisher Scientific, Waltham, MA) for 30 minutes at 37 °C and then washed and resuspended with culture medium. Cells were counted with Countess 2 (Thermo Fisher Scientific, Waltham, MA) and diluted to 10^4 cells per mL with culture medium. After dilution,

the exact number of cells was confirmed with Nageotte counting chamber (Hausser Scientific, Horsham, PA). Variable number (10, 50, 100, and 200) of cancer cells were spiked into 0.015% (v/v) ferrofluid for spiking experiments.

Recovery rate and purity calculation of i²FCS

Cells collected from the CTC outlet and WBC outlet were stained with 2 μM DAPI (Thermo Fisher Scientific, Waltham, MA) to stain cell nucleus, and counted with a Nageotte counting chamber. Cells with CellTracker (Green/Orange) signal were identified as cancer cells, while other cells only expressing DAPI signal were identified as WBCs. The recovery rate of i²FCS was calculated by $\left(N_{cancer\_cell@CTC\_outlet} \middle/ \left(N_{cancer\_cell@CTC\_outlet} + N_{cancer\_cell@WBC\_outlet}\right)\right) \times 100\%$. The purity was characterized by the WBC carryover $N_{WBC@CTC\_outlet}$, the depletion rate $\left(1 - N_{WBC@CTC\_outlet} \middle/ N_{Total\_WBC}\right) \times 100\%$, and the log depletion rate $\log\left(N_{Total\_WBC} \middle/ N_{WBC@CTC\_outlet}\right)$.

Cell morphology characterization

Cells suspended in PBS were deposited on a microscope slide and imaged with an inverted microscope (Axio Observer, Carl Zeiss, Germany) in bright field mode. Cell morphologies were analyzed with ImageJ software. Effective cell diameter was measured as the maximum Feret diameter of the cells under bright-field imaging.

Cell viability and proliferation characterization

Short-term cell viability of lung cancer cell line H1299 after i²FCS processing was characterized with a Live/Dead assay (Thermo Fisher Scientific, Waltham, MA) following the manufacturer's protocol. All cells are alive at the start of the viability characterization. Dead cells and cell debris were removed by PBS wash after cell culture. For long-term proliferation,

the isolated H1299 cells from i^{2}FCS device were washed three times with cell culture medium to remove the ferrofluid, and then the cells were re-suspended with culture medium and transferred into a T25 flask. (Corning, Corning, NY). The cells were then cultured at 37°C (5% CO_2) under a humidified atmosphere. Cellular morphology was inspected every 24 hours.

Live subject statement

All experiments in this study were performed in compliance with the regulations of the United States Office for Human Research Protections, and the University of Georgia Human Subjects Office. Human whole blood collected from healthy donors was purchased from company (ZenBio, Durham, NC) for spiking experiments. Cancer patient blood was obtained from the University Cancer and Blood center, LLC (Athens, GA) following a protocol approved by the Institutional Review Board (IRB) at the University of Georgia (VERSION00000869). Informed consent was obtained for cancer patient participants.

Human sample processing

Complete blood count (CBC) reports of cancer patients' blood samples were used to determine the number of WBCs to optimize WBC labeling. Whole blood was firstly labeled with biotinylated antibodies including anti-CD45 (eBioscience, San Diego, CA), anti-CD45RA (eBioscience, San Diego, CA), anti-16 (eBioscience, San Diego, CA), anti-66b (Biolegend, San Diego, CA), and anti-CD3 (Biolegend, San Diego, CA) for 30 minutes at room temperature. The antibody-conjugated blood was lysed with RBC lysis buffer (eBioscience, San Diego, CA) for 5 minutes following by centrifugation (500g, 5 minutes) at room temperature. After removing the supernatant, the cells were resuspended with 1× PBS and incubated with washed Dynabeads (Thermo Fisher Scientific, Waltham, MA) for 30 minutes on a rocker. All the labeling and washing procedures were performed following the manufacturer's protocol. Blood cells were suspended in the same volume of 0.015% (v/v) ferrofluid supplemented with 0.1%

(v/v) Pluronic F-68 surfactant (Thermo Fisher Scientific, Waltham, MA) before processing using the device.

CTC identification

After device processing, isolated cells were concentrated through centrifugation (600g, 5 minutes) and immobilized onto poly-L-lysine (Sigma-Aldrich, St. Louis, Mo) coated glass slides. Isolated cells were fixed with 4% (w/v) paraformaldehyde (Santa Cruz Biotechnology, Dallas, TX) for 10 minutes and subsequently permeabilized with 0.1% (v/v) Triton X-100 (Alfa Aesar, Haverhill, MA) in PBS for 10 minutes at room temperature. Cells were then blocked with Ultracruz blocking reagent (Santa Cruz Biotechnology, Dallas, TX) for 30 minutes at room temperature to block nonspecific binding sites. Cells were then immunostained overnight at 4 °C with primary antibodies including EpCAM-Alexa Fluor 488, N-cadherin-Alex Fluor 594, Vimentin-Alex Fluor 647 (Santa Cruz Biotechnology, Dallas, TX), CD45-PE (BD Bioscience, San Jose, CA). Cells were stored in mounting medium supplemented with DAPI (Fluoroshield^{TM} with DAPI, Sigma-Aldrich, St. Louis, Mo).

Migration assay of isolated CTCs

Isolated CTCs were loaded into a microfluidic migration device for single cell migration assay.10% Fetal Bovine Serum (FBS, Thermo Fisher Scientific, Waltham, MA), 20 ng mL^{-1} epidermal growth factor (EGF, Thermo Fisher Scientific, Waltham, MA), and 20 ng mL^{-1} basic fibroblast growth factor (bFGF, Thermo Fisher Scientific, Waltham, MA) were used as the chemoattractants for the CTCs, while 5 µg mL^{-1} Slit2 (Thermo Fisher Scientific, Waltham, MA) was used to inhibit the migration of WBCs. After cell loading, migration assay was performed in an incubator (37 °C, 5% CO_2) for 24 hours. Cells was immunofluorescently stained in the device to identify their cell types.

Authors' contribution

L.M. conceived the study and supervised research. Y.L. designed the i^{2}FCS and single cell migration device and its research. Y.L. performed experiments. L.M. and Y.L. analyzed data. W.Z. assisted in the device setup. R.C. assisted in the modeling and simulation. J.H., M.E., C.N.C.P, P.G.N. aided with the cancer patients' recruitment and obtaining samples. Y.L. and L.M. wrote the manuscript with inputs from all the authors.

Conflicts of interest

i^{2}FCS and single cell migration device are the subject of the United States utility patent applications. Intellectual property related to i^{2}FCS and single cell migration device is owned by the University of Georgia Research Foundation. Leidong Mao founded and owned FCS Technology LLC to commercialize i^{2}FCS and single cell migration device. Leidong Mao and Wujun Zhao have financial interests in FCS Technology LLC, which is subject to certain restrictions under the university policy. The terms of this arrangement are being managed by the University of Georgia in accordance with its conflict of interest policies.

Acknowledgments

We are grateful for the donors of blood samples for this study. This study is supported by the National Science Foundation under Grant Nos. 1150042, 1659525 and 1648035, the National Center for Advancing Translational Sciences of the National Institutes of Health under Award No. UL1TR002378, and the National Institute of Biomedical Imaging and Bioengineering of the National Institutes of Health under Award No. 1R41EB028191-01. The content is solely the responsibility of the authors and does not necessarily represent the official views of the National Institutes of Health.

Table 1. Comparison of design, operation and performance of CTC isolation between CTC-iChip and i²FCS.

Technology	Blood processing throughput (mL h^{-1})	CTC recovery rate (spiked cell lines)	White blood cells (WBC) carryover at device outlets	Recovered patient CTCs diameter range	Cell viability (cell lines)	Design and operation	Red blood cell lysis needed?
CTC-iChip[35]	8	~ 97%	32,000 WBCs/mL	>9 μm	Not reported	Integration of DLD, inertial focusing and magnetophoresis in two devices.	No
Monolithic CTC-iChip[36]	~10	~99.5%	445 WBCs/mL	5.5-27 μm	Not reported	Integration of DLD, inertial focusing and magnetophoresis in a single device.	No
i²FCS (this paper)	60	99.7%	507 WBCs/mL	4.3-33.7 μm	98.10%	Integration of inertial focusing and ferrohydrodynamic separation in a single device.	Yes

References:

1. M. Poudineh, E. H. Sargent, K. Pantel and S. O. Kelley, *Nat Biomed Eng*, 2018, **2**, 72-84.

2. C. Alix-Panabieres and K. Pantel, *Nature Biomedical Engineering*, 2017, **1**.

3. J. Massague and A. C. Obenauf, *Nature*, 2016, **529**, 298-306.

4. M. G. Krebs, R. L. Metcalf, L. Carter, G. Brady, F. H. Blackhall and C. Dive, *Nat Rev Clin Oncol*, 2014, **11**, 129-144.

5. E. Heitzer, I. S. Haque, C. E. S. Roberts and M. R. Speicher, *Nat Rev Genet*, 2019, **20**, 71-88.

6. N. Ma and S. S. Jeffrey, *Science*, 2020, **367**, 1424-1425.

7. S. Riethdorf, H. Fritsche, V. Muller, T. Rau, C. Schindibeck, B. Rack, W. Janni, C. Coith, K. Beck, F. Janicke, S. Jackson, T. Gornet, M. Cristofanilli and K. Pantel, *Clinical Cancer Research*, 2007, **13**, 920-928.

8. A. Romiti, S. Raffa, R. Di Rocco, M. Roberto, A. Milano, A. Zullo, L. Leone, D. Ranieri, F. Mazzetta, E. Medda, I. Sarcina, V. Barucca, C. D'Antonio, V. Durante, M. Ferri, M. R. Torrisi and P. Marchetti, *J Gastrointest Liver*, 2014, **23**, 279-284.

9. F. C. Bidard, D. J. Peeters, T. Fehm, F. Nole, R. Gisbert-Criado, D. Mavroudis, S. Grisanti, D. Generali, J. A. Garcia-Saenz, J. Stebbing, C. Caldas, P. Gazzaniga, L. Manso, R. Zamarchi, A. F. de Lascoiti, L. De Mattos-Arruda, M. Ignatiadis, R. Lebofsky, S. J. van Laere, F. Meier-Stiegen, M. T. Sandri, J. Vidal-Martinez, E. Politaki, F. Consoli, A. Bottini, E. Diaz-Rubio, J. Krell, S. J. Dawson, C. Raimondi, A. Rutten, W. Janni, E. Munzone, V. Caranana, S. A. Agelaki, C. Almici, L. Dirix, E. F. Solomayer, L. Zorzino, H. Johannes, J. S. Reis, K. Pantel, J. Y. Pierga and S. Michiels, *Lancet Oncol*, 2014, **15**, 406-414.

10. A. W. Lambert, D. R. Pattabiraman and R. A. Weinberg, *Cell*, 2017, **168**, 670-691.

11. C. L. Chaffer and R. A. Weinberg, *Science*, 2011, **331**, 1559-1564.

12. M. Poudineh, P. Aldridge, S. Ahmed, B. J. Green, L. Kermanshah, V. Nguyen, C. Tu, R. M. Mohamadi, R. K. Nam, A. Hansen, S. S. Sridhar, A. Finelli, N. E. Fleshner, A. M. Joshua, E. H. Sargent and S. O. Kelley, *Nat Nanotechnol*, 2017, **12**, 274-+.

13. Y. H. Cheng, Y. C. Chen, E. Lin, R. Brien, S. Jung, Y. T. Chen, W. Lee, Z. Hao, S. Sahoo, H. Min Kang, J. Cong, M. Burness, S. Nagrath, S. W. M and E. Yoon, *Nat Commun*, 2019, **10**, 2163.

14. E. Sahai, *Nat Rev Cancer*, 2007, **7**, 737-749.

15. L. Keller and K. Pantel, *Nat Rev Cancer*, 2019, **19**, 553-567.

16. B. Strilic and S. Offermanns, *Cancer Cell*, 2017, **32**, 282-293.

17. P. S. Steeg, *Nature reviews cancer*, 2016, **16**, 201-218.

18. P. Friedl and K. Wolf, *Nat Rev Cancer*, 2003, **3**, 362-374.

19. C. D. Paul, P. Mistriotis and K. Konstantopoulos, *Nat Rev Cancer*, 2017, **17**, 131-140.

20. C. Alix-Panabieres and K. Pantel, *Nat Rev Cancer*, 2014, **14**, 623-631.

21. M. Poudineh, E. H. Sargent, K. Pantel and S. O. Kelley, *Nat Biomed Eng*, 2018, **2**, 72-84.

22. C. Alix-Panabieres, K. Bartkowiak and K. Pantel, *Mol Oncol*, 2016, **10**, 443-449.

23. Y. Zhang, W. Zhang and L. Qin, *Angew Chem Int Ed Engl*, 2014, **53**, 2344-2348.

24. C. L. Yankaskas, K. N. Thompson, C. D. Paul, M. I. Vitolo, P. Mistriotis, A. Mahendra, V. K. Bajpai, D. J. Shea, K. M. Manto, A. C. Chai, N. Varadarajan, A. Kontrogianni-Konstantopoulos, S. S. Martin and K. Konstantopoulos, *Nat Biomed Eng*, 2019, **3**, 452-465.

25. Y. C. Chen, S. G. Allen, P. N. Ingram, R. Buckanovich, S. D. Merajver and E. Yoon, *Sci Rep*, 2015, **5**, 9980.

26. I. Y. Wong, S. Javaid, E. A. Wong, S. Perk, D. A. Haber, M. Toner and D. Irimia, *Nat Mater*, 2014, **13**, 1063-1071.

27. M. Poudineh, M. Labib, S. Ahmed, L. N. Nguyen, L. Kermanshah, R. M. Mohamadi, E. H. Sargent and S. O. Kelley, *Angew Chem Int Ed Engl*, 2017, **56**, 163-168.

28. D. Di Carlo, D. Irimia, R. G. Tompkins and M. Toner, *Proc Natl Acad Sci U S A*, 2007, **104**, 18892-18897.

29. H. Amini, W. Lee and D. Di Carlo, *Lab Chip*, 2014, **14**, 2739-2761.

30. D. Di Carlo, *Lab Chip*, 2009, **9**, 3038-3046.

31. R. E. Rosensweig, *Ferrohydrodynamics*, Cambridge University Press, Cambridge, 1985.

32. W. Zhao, Y. Liu, B. D. Jenkins, R. Cheng, B. N. Harris, W. Zhang, J. Xie, J. R. Murrow, J. Hodgson, M. Egan, A. Bankey, P. G. Nikolinakos, H. Y. Ali, K. Meichner, L. A. Newman, M. B. Davis and L. Mao, *Lab Chip*, 2019, **19**, 1860-1876.

33. Y. Liu, W. Zhao, R. Cheng, B. N. Harris, J. R. Murrow, J. Hodgson, M. Egan, A. Bankey, P. G. Nikolinakos, T. Laver, K. Meichner and L. Mao, *Lab Chip*, 2021, DOI: 10.1039/d1lc00119a.

34. A. Mishra, T. D. Dubash, J. F. Edd, M. K. Jewett, S. G. Garre, N. M. Karabacak, D. C. Rabe, B. R. Mutlu, J. R. Walsh and R. Kapur, *Proceedings of the National Academy of Sciences*, 2020, **117**, 16839-16847.

35. E. Ozkumur, A. M. Shah, J. C. Ciciliano, B. L. Emmink, D. T. Miyamoto, E. Brachtel, M. Yu, P. I. Chen, B. Morgan, J. Trautwein, A. Kimura, S. Sengupta, S. L. Stott, N. M. Karabacak, T. A. Barber, J. R. Walsh, K. Smith, P. S. Spuhler, J. P. Sullivan, R. J. Lee, D. T. Ting, X. Luo, A. T. Shaw, A. Bardia, L. V. Sequist, D. N. Louis, S. Maheswaran, R. Kapur, D. A. Haber and M. Toner, *Science Translational Medicine*, 2013, **5**, 179ra147.

36. F. Fachin, P. Spuhler, J. M. Martel-Foley, J. F. Edd, T. A. Barber, J. Walsh, M. Karabacak, V. Pai, M. Yu, K. Smith, H. Hwang, J. Yang, S. Shah, R. Yarmush, L. V. Sequist, S. L. Stott, S. Maheswaran, D. A. Haber, R. Kapur and M. Toner, *Sci Rep*, 2017, **7**, 10936.

37. M. A. Nieto, R. Y. Huang, R. A. Jackson and J. P. Thiery, *Cell*, 2016, **166**, 21-45.

38. J. P. Thiery, H. Acloque, R. Y. Huang and M. A. Nieto, *Cell*, 2009, **139**, 871-890.

39. J. P. Thiery, *Nat Rev Cancer*, 2002, **2**, 442-454.

40. Y. Liu, W. Zhao, R. Cheng, A. Puig, J. Hodgson, M. Egan, C. N. Cooper Pope, P. G. Nikolinakos and L. Mao, *Lab Chip*, 2021, **21**, 2738-2750.

41. J. J. Nieva and P. Kuhn, *Future Oncology*, 2012, **8**, 989-998.

42. D. J. Peeters, G. G. Van den Eynden, P. J. van Dam, A. Prove, I. H. Benoy, P. A. van Dam, P. B. Vermeulen, P. Pauwels, M. Peeters, S. J. Van Laere and L. Y. Dirix, *Br J Cancer*, 2011, **104**, 1472-1477.

43. R. A. Harouaka, M. Nisic and S. Y. Zheng, *J Lab Autom*, 2013, **18**, 455-468.

44. D. Marrinucci, K. Bethel, D. Lazar, J. Fisher, E. Huynh, P. Clark, R. Bruce, J. Nieva and P. Kuhn, *J Oncol*, 2010, **2010**, 861341.

45. M. Yu, A. Bardia, B. Wittner, S. L. Stott, M. E. Smas, D. T. Ting, S. J. Isakoff, J. C. Ciciliano, M. N. Wells, A. M. Shah, K. F. Concannon, M. C. Donaldson, L. V. Sequist, E. Brachtel, D. Sgroi, J. Baselga, S. Ramaswamy, M. Toner, D. A. Haber and S. Maheswaran, *Science*, 2013, **339**, 580-584.

46. S. L. Stott, C.-H. Hsu, D. I. Tsukrov, M. Yu, D. T. Miyamoto, B. A. Waltman, S. M. Rothenberg, A. M. Shah, M. E. Smas, G. K. Korir, F. P. Floyd, A. J. Gilman, J. B. Lord, D. Winokur, S. Springer, D. Irimia, S. Nagrath, L. V. Sequist, R. J. Lee, K. J. Isselbacher, S. Maheswaran, D. A. Haber and M. Toner, *Proceedings of the National Academy of Sciences*, 2010, **107**, 18392-

18397.

47. R. J. Petrie, A. D. Doyle and K. M. Yamada, *Nat Rev Mol Cell Biol*, 2009, **10**, 538-549.

48. E. T. Roussos, M. Balsamo, S. K. Alford, J. B. Wyckoff, B. Gligorijevic, Y. Wang, M. Pozzuto, R. Stobezki, S. Goswami, J. E. Segall, D. A. Lauffenburger, A. R. Bresnick, F. B. Gertler and J. S. Condeelis, *J Cell Sci*, 2011, **124**, 2120-2131.

49. E. T. Roussos, J. S. Condeelis and A. Patsialou, *Nat Rev Cancer*, 2011, **11**, 573-587.

50. J. Y. Wu, L. Feng, H. T. Park, N. Havlioglu, L. Wen, H. Tang, K. B. Bacon, Z. Jiang, X. Zhang and Y. Rao, *Nature*, 2001, **410**, 948-952.

51. L. Boneschansker, J. Yan, E. Wong, D. M. Briscoe and D. Irimia, *Nat Commun*, 2014, **5**, 4787.

52. K. Wolf, S. Alexander, V. Schacht, L. M. Coussens, U. H. von Andrian, J. van Rheenen, E. Deryugina and P. Friedl, *Semin Cell Dev Biol*, 2009, **20**, 931-941.

53. B. Weigelin, G. J. Bakker and P. Friedl, *Intravital*, 2012, **1**, 32-43.

54. P. C. Benias, R. G. Wells, B. Sackey-Aboagye, H. Klavan, J. Reidy, D. Buonocore, M. Miranda, S. Kornacki, M. Wayne, D. L. Carr-Locke and N. D. Theise, *Sci Rep*, 2018, **8**, 4947.

55. E. Sahai, *Curr Opin Genet Dev*, 2005, **15**, 87-96.

56. K. Wolf, I. Mazo, H. Leung, K. Engelke, U. H. von Andrian, E. I. Deryugina, A. Y. Strongin, E. B. Brocker and P. Friedl, *J Cell Biol*, 2003, **160**, 267-277.

57. E. Sahai and C. J. Marshall, *Nat Cell Biol*, 2003, **5**, 711-719.

58. W. J. Zhao, R. Cheng, S. H. Lim, J. R. Miller, W. Z. Zhang, W. Tang, J. Xie and L. D. Mao, *Lab on a Chip*, 2017, **17**, 2243-2255.

59. Y. Liu, W. Zhao, R. Cheng, M. Logun, M. D. M. Zayas-Viera, L. Karumbaiah and L. Mao, *Lab Chip*, 2020, **20**, 3187-3201.

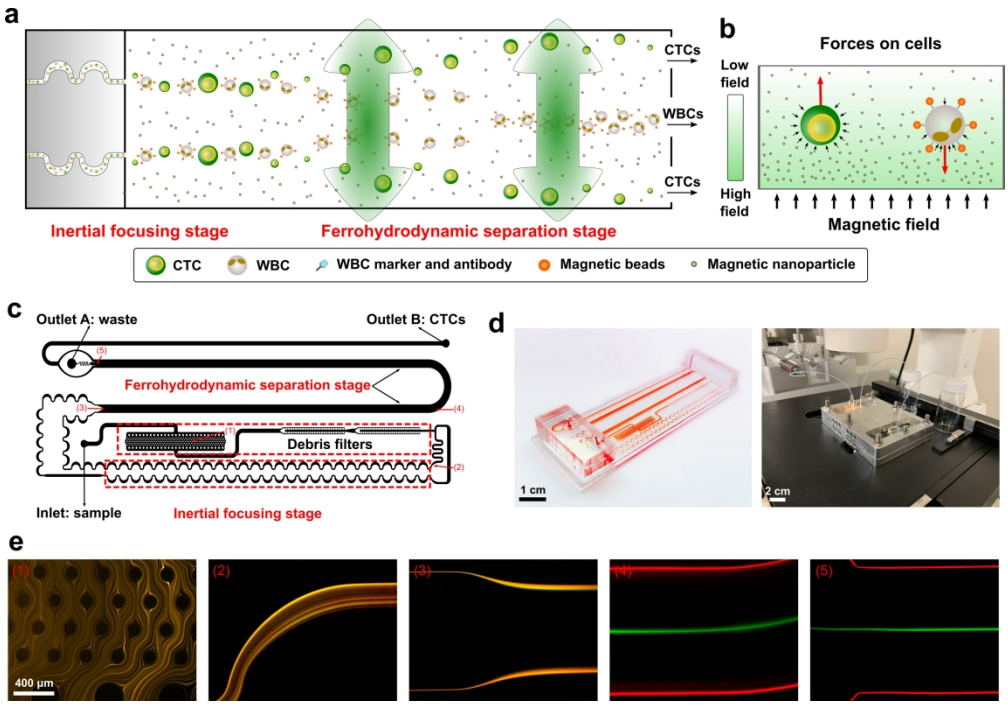

Figure 1. Overview of the integrated inertial ferrohydrodynamic cell separation (i2FCS) scheme and its device.

252x174mm (300 x 300 DPI)

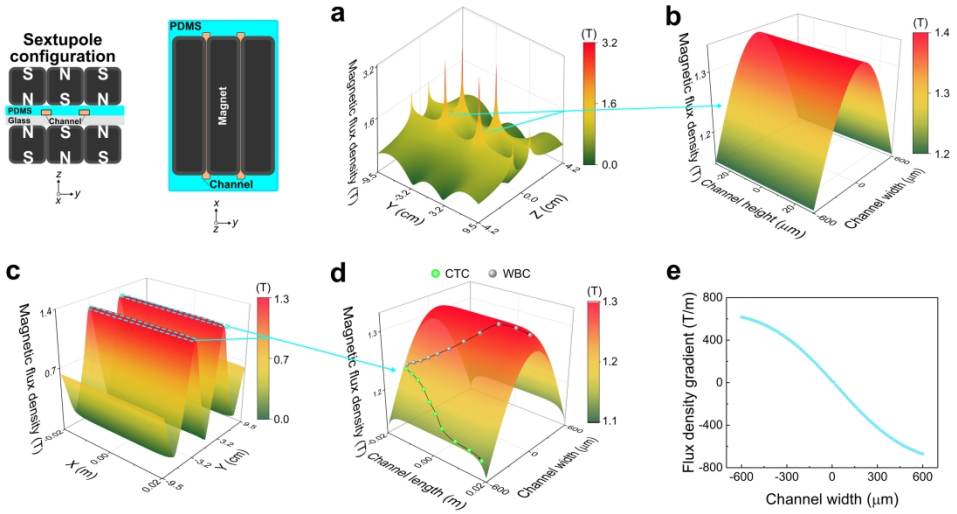

Figure 2. Optimization of the magnetic field to achieve high magnetic flux density and flux density gradient in the i2FCS device.

255x131mm (300 x 300 DPI)

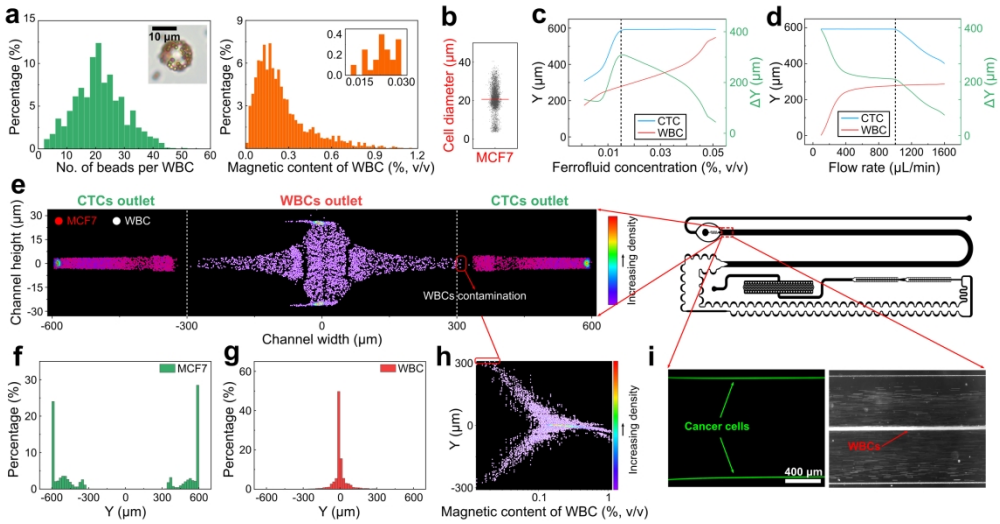

Figure 3. System optimization of i2FCS devices for the isolation of CTCs (down to 10 cells per mL) with high recovery rate, low WBC contamination, and ultrahigh throughput.

255x133mm (300 x 300 DPI)

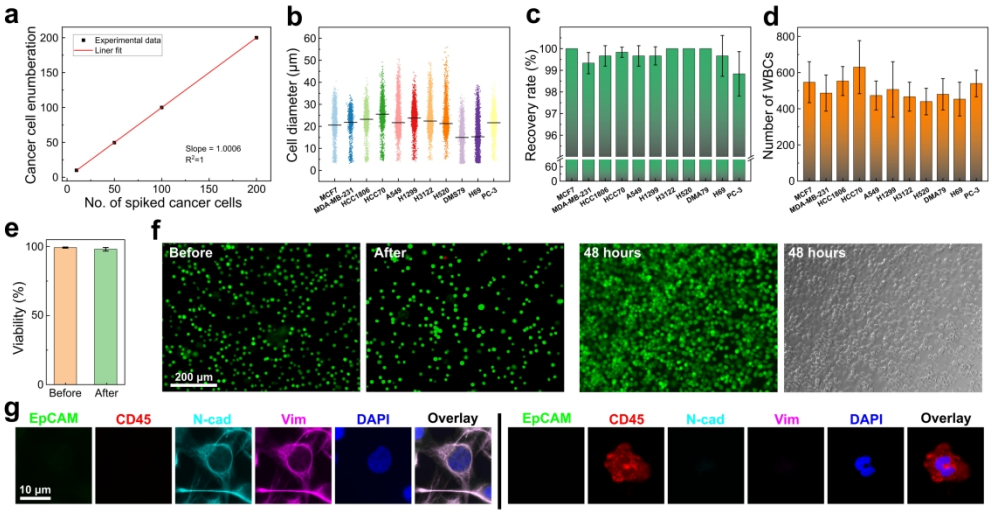

Figure 4. Characterization of i2FCS device performance using cancer cell lines spiked into blood from healthy donors. Cancer cells and WBCs were processed in 0.015% (v/v) ferrofluid with a flow rate of 1000 μL min-1 (60 mL h-1) to achieve high cancer cell recovery rate and low WBC contamination.

254x129mm (300 x 300 DPI)

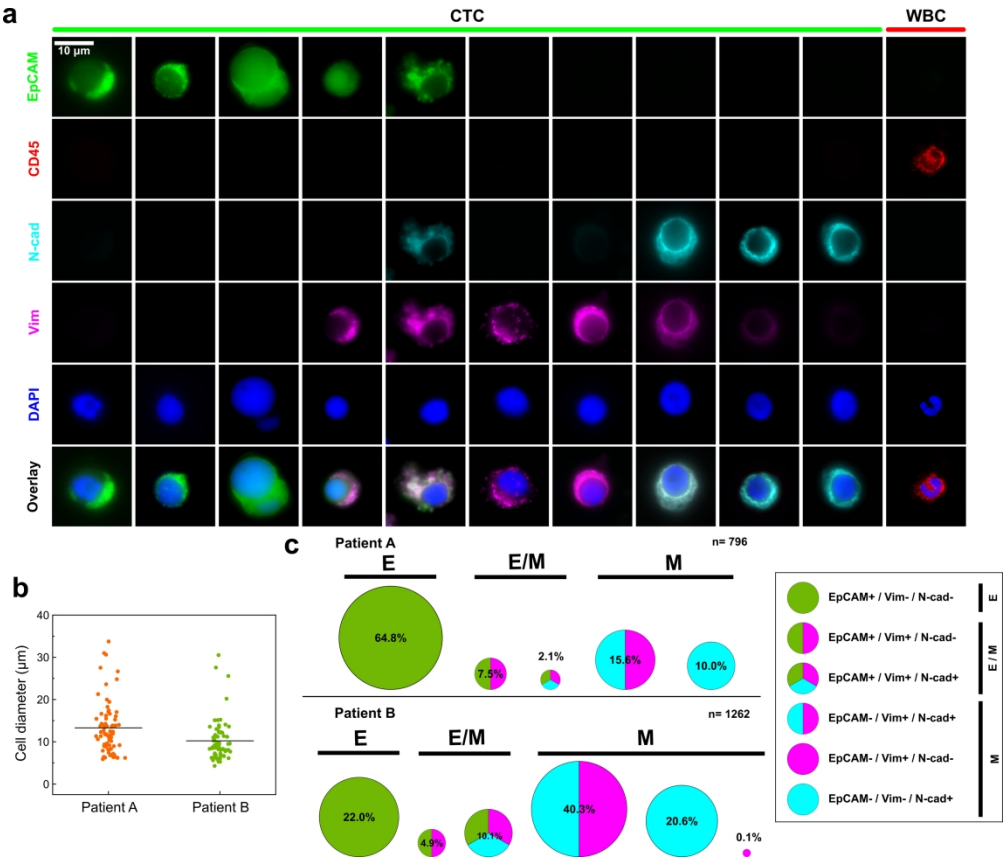

Figure 5. Biochemical phenotyping of CTCs isolated from two metastatic lung cancer patients (n = 2).

250x212mm (300 x 300 DPI)

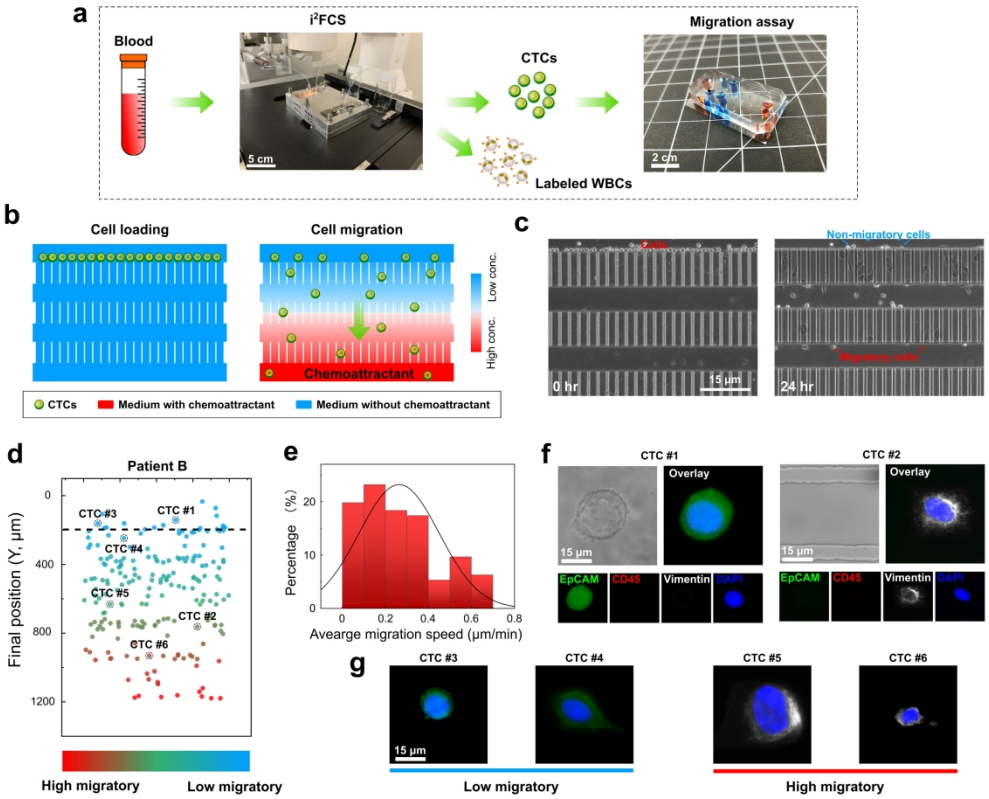

Figure 6. Functional phenotyping of CTCs isolated from one metastatic lung cancer patient (n = 1).

254x202mm (300 x 300 DPI)